Journal of Power Sources 213 (2012) 55–62

Contents lists available at SciVerse ScienceDirect

Journal of Power Sources

journal homepage: www.elsevier.com/locate/jpowsour

Properties and electrochemical performance of $La_{0.75}Sr_{0.25}Cr_{0.5}Mn_{0.5}O_{3-\delta}$–$La_{0.2}Ce_{0.8}O_{2-\delta}$ composite anodes for solid oxide fuel cells

Manas K. Rath [a], Byung-Hyun Choi [c], Ki-Tae Lee [a,b,*]

[a] Division of Advanced Materials Engineering, Chonbuk National University, Jeonbuk 561-756, South Korea
[b] Hydrogen and Fuel Cell Research Center, Chonbuk National University, Jeonbuk 561-756, South Korea
[c] Optic and Electronic Ceramics Division, Korea Institute of Ceramic Engineering and Technology, Seoul 153-801, South Korea

ARTICLE INFO

Article history:
Received 11 February 2012
Received in revised form
28 March 2012
Accepted 31 March 2012
Available online 19 April 2012

Keywords:
Solid oxide fuel cells
Perovskite
Sol–gel
Oxide anodes
Carbon deposition

ABSTRACT

Highly crystalline composite anodes composed of $La_{0.75}Sr_{0.25}Cr_{0.5}Mn_{0.5}O_{3-\delta}$–$La_{0.2}Ce_{0.8}O_{2-\delta}$ (LSCM–LDC) have been synthesized using a simple modified sol–gel method. LSCM is known for its superior redox stability. LDC acts both as an agent that blocks grain growth in LSCM, and reduces the area-specific resistance of the electrode, thereby enhancing the overall electrochemical performance of single cells. However, the carbon deposition rate of LSCM–LDC composite anodes increases with increasing LDC content. The optimal anode composition is 50 wt.% LSCM–50 wt.% LDC. This composite has a polarization resistance of 0.081 Ω cm^2 and 0.130 Ω cm^2 in H_2 and CH_4, respectively, measured at 800 °C.

1. Introduction

Solid oxide fuel cells (SOFCs) are promising energy-harvesting devices because they are environmentally friendly, have a high energy conversion efficiency, demonstrate multi-fuel capability, and are modular [1,2]. The distinguishing feature of SOFCs is that they feature good oxygen anion transports from the cathode to the anode through a highly dense oxide electrolyte; oxidation of fuel occurs at the interface of the anode and the electrolyte, which is called the triple phase boundary (TPB). In conventional SOFCs operated with hydrogen fuel, highly dense 8 mol% Y_2O_3-stabilized ZrO_2 (YSZ), Ni-YSZ cermet, and $La_{0.6}Sr_{0.4}MnO_3$ (LSM) function as the electrolyte, anode, and cathode, respectively.

However, in the case of hydrocarbon-fueled SOFCs, the conventional Ni-YSZ cermet anode has poor durability due to the formation of coke from the hydrocarbon fuel, which degrades the cell performance and stability [1,2]. To overcome this drawback, several advanced oxide anodes have been investigated. Among these, $La_{0.75}Sr_{0.25}Cr_{0.5}Mn_{0.5}O_{3-\delta}$ (LSCM) exhibits excellent redox stability characteristics [3–5]. This LSCM anode is a member of the $La_{1-x}A_xCr_{1-y}M_yO_{3-\delta}$ perovskite family (A = alkaline earth and B = transition metal). $La_{1-x}A_xCr_{1-y}M_yO_{3-\delta}$ perovskite anodes are ideal for use in hydrocarbon-fuel cell applications because they show substantial electrochemical activity in reducing and oxidizing atmospheres, are compatible with various solid electrolytes, and display good dimensional stability despite phase changes upon reduction [6]. It has been reported that in a reducing atmosphere, no substantial weight loss occurs because the B-site 'Cr' retains its six-fold coordination chemistry (no oxygen vacancies). Hence, it is necessary to introduce M = Mn, Fe, Co, Ni, and other metals to generate oxygen vacancies. In the case of $La_{1-x}A_xCr_{1-y}M_yO_{3-\delta}$, Cr-rich solid solutions exhibit low electronic transport capacity at reduced $P(O_2)$. While iron-containing materials (M = Fe) suffer from excessive chemically induced expansion and phase decomposition under anodic conditions [4,7–15], 'Mn' doping at the B-site enhances the catalytic properties and ionic conductivity of perovskite LSCM anodes [5,16–20].

To enhance the catalytic activity and reduce the polarization loss of perovskite LSCM anodes, the anodes can be impregnated or be used to create composites with electrolyte materials. Tao and

* Corresponding author. Division of Advanced Materials Engineering, Chonbuk National University, Jeonbuk 561-756, South Korea. Tel.: +82 63 270 2290; fax: +82 63 270 2386.
E-mail address: ktlee71@jbnu.ac.kr (K.-T. Lee).

0378-7753/$ – see front matter © 2012 Elsevier B.V. All rights reserved.
doi:10.1016/j.jpowsour.2012.03.105

Irvine reported that the polarization resistance of LSCMs was 0.26 Ω cm^2 in wet H_2 and 0.87 Ω cm^2 in wet CH_4 at 900 °C, respectively [3]. Several approaches to the reduce polarization loss (polarization resistance, R_P) have also been evaluated. The polarization resistance of an LSCM–YSZ composite anode that was synthesized by a gel-casting method was 0.46 Ω cm^2 at 800 °C under H_2 fuel [13]. Impregnation of $Ce_{0.9}Gd_{0.1}O_{2-\delta}$ (GDC) into the porous LSCM anode reduced the polarization resistance. The resistance values were 0.12 and 0.44 Ω cm^2 in wet H_2 and wet CH_4, respectively [21]. Chen et al. reported that an LSCM (33 wt.%)–GDC (67 wt.%) composite anode synthesized by a combined citrate and EDTA method exhibited polarization resistance values of 0.146 Ω cm^2 and 0.496 Ω cm^2 in wet H_2 and in wet CH_4, respectively, at 800 °C [5].

Meanwhile, $La_{0.2}Ce_{0.8}O_{2-\delta}$ (LDC), which has higher oxide ion conductivity than YSZ, also shows electronic conduction due to the reduction of Ce^{4+} to Ce^{3+} at low oxygen partial pressures [22,23]. In contrast to GDC, LDC could inhibit the grain growth of LSCM at high temperatures by functioning as a diffusion barrier. Huang et al. described using LDC as a buffer layer to suppress the interdiffusion of ionic species between a $La_{0.8}Sr_{0.2}Ga_{0.8}Mg_{0.2}O_3$ (LSGM) electrolyte and an Ni-YSZ anode [24].

We generated composite anodes comprised of $La_{0.75}Sr_{0.25}Cr_{0.5}Mn_{0.5}O_{3-\delta}$–$La_{0.2}Ce_{0.8}O_{2-\delta}$ (LSCM–LDC) to enhance the catalytic activity and reduce the polarization loss of the anode in a hydrocarbon fuel system. Furthermore, we investigated the electrochemical properties and carbon deposition behaviors of LSCM–LDC composites with different weight ratios.

2. Experimental procedures

2.1. Powder synthesis

LSCM–LDC composite powders with different weight ratios were synthesized by a modified combustion technique using sucrose. The raw materials used in this study were $La(NO_3)_2 \cdot xH_2O$ (Aldrich, 99.9%), $Sr(NO_3)_3$ (Alfa Aesar, 99.0%), $Cr(NO_3)_2 \cdot 9H_2O$ (Alfa Aesar, 98.5%), and $Mn(NO_3) \cdot 4H_2O$ (Alfa Aesar, 98%). Sucrose (Alfa Aesar, 99%) and pectin (Aldrich) were used as the fuel and catalyst, respectively, for the combustion process. The combustion techniques are described in Fig. 1.

The composite cathode powder of $Ba_{0.5}S_{r0.5}Co_{0.2}Fe_{0.8}O_{3-\delta}$–$Gd_{0.2}Ce_{0.8}O_{2-\delta}$ was also prepared using a sucrose-modified sol–gel technique. The raw materials for the powder processing were $Ba(NO_3)_2$ (Alfa Aesar, 99%), $Sr(NO_3)_2$ (Alfa Aesar, 99.0%), $Co(NO_3)_3 \cdot 6H_2O$ (Aldrich, 98%+ ACS), $Fe(NO_3)_3 \cdot 9H_2O$ (Alfa Aesar, 98%∼, Alfa Aesar), $Ce(NO_3)_3 \cdot 6H_2O$ (Aldrich, 99% metal basis), and $Gd(NO_3)_3 \cdot xH_2O$ (x ∼6, Alfa Aesar, 99.9%, REO). The powder processing techniques used were similar to those mentioned for the anode materials.

2.2. Materials characterization

The synthesized composite anodes were characterized by X-ray diffraction (XRD) using Cu-Kα radiation for phase analysis. The morphology and elementary analysis results for the powders were evaluated by field emission scanning electron microscopy (FE-SEM, JSM-6400, JEOL, Japan). The specific surface area and particle size of each powder was measured by BET (Brunauer, Emmett, Teller) analysis (ASAP2010 physisorption analyzer, Micrometrics, USA) and by dynamic light scattering method (ELS 6000 zeta potential and particle size analyzer, Otsuka Electronics, Japan), respectively. The chemical stability of the as-synthesized anode materials with YSZ and GDC electrolytes was investigated by X-ray diffraction. To evaluate the carbon deposition behavior of the powders, thermogravimetric analysis (TGA) was performed. First, LSCM–LDC composites were placed in a clean alumina crucible and heated at 750 °C for 6 h with a CH_4 at flow rate of 100 cm^3 min^{-1}. Subsequently, the powders were analyzed by TGA (TA Q600, TA instruments, USA) in air over the temperature range of 30 °C–1000 °C at a heating rate of 10 °C min^{-1}. Weight loss graphs were subsequently analyzed.

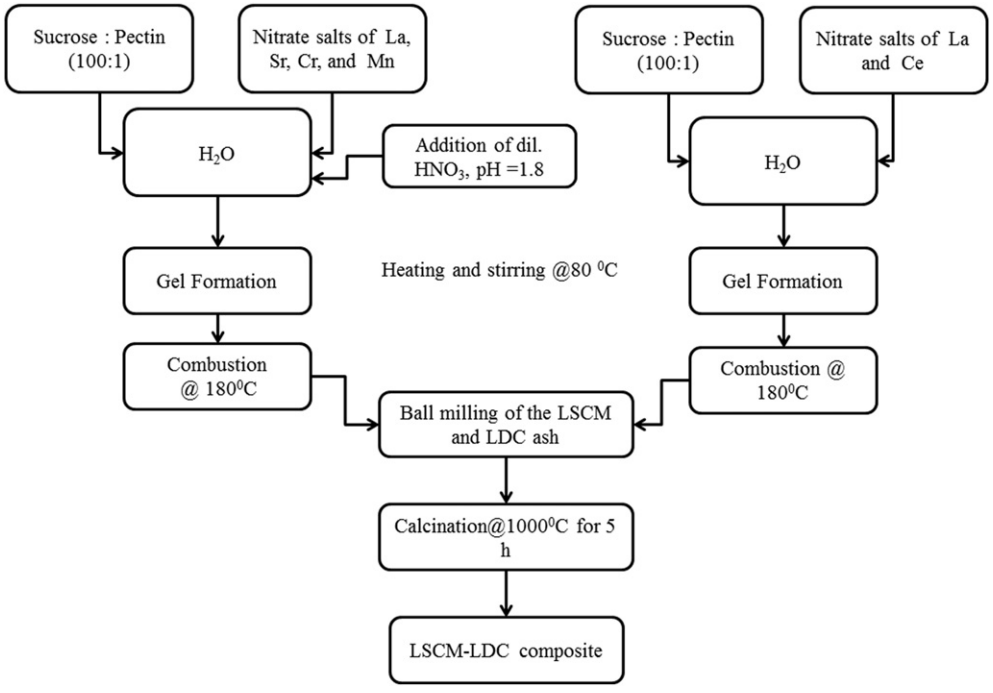

Fig. 1. Flow chart for the synthesis of LSCM–LDC composite powders using a modified sol–gel combustion technique.

2.3. Electrochemical performance tests

Electrochemical performance was evaluated with electrolyte-supported single cells. Commercial GDC powder (CGO90/10 UHSA, Grand C&M Co. Ltd.) was compressed by cold iso-static pressing (CIP) and subsequently fired at 1450 °C for 4 h to fabricate a 0.5-mm thick GDC electrolyte pellet. An LSCM–LDC composite anode layer was screen-printed onto the GDC pellets and the pellets were fired at 1250 °C for 5 h. In the same manner, the BSCF–GDC cathode layer was screen-printed onto the other side of the GDC pellets in a symmetric position followed by firing at 1050 °C for 2 h. The geometric area of both electrodes was 0.25 cm^2. Finally, the Pt mesh was used as a current collector. AC impedance analysis was performed using a universal potentiostat with a frequency response analyzer (Bio-logic science instrument) with a three-electrode configuration under humidified H_2 and CH_4 at 700 °C, 750 °C, and 800 °C. The applied frequency was in the range of 0.1 mHz–1 MHz with a voltage amplitude of 10 mV. Current–voltage (I–V) measurements of single cells were also performed using the three-electrode configuration. A Pt mesh placed onto the electrode with a spring-loaded alumina tube was used as the current corrector. A seal between the single cell and the alumina tube was achieved with a Pyrex® glass ring. Humidified H_2 (~3% H_2O at 30 °C) and air were supplied as fuel and oxidant, respectively, at a rate of 100 cm^3 min^{-1}. To verify hydrocarbon fuel use, humidified CH_4 was also used as fuel.

3. Results and discussion

3.1. Phase and morphology analysis

The XRD patterns of all composite anodes that were calcined at 1000 °C, along with pure LSCM (100LSCM) and pure LDC are shown in Fig. 2. For convenience, we denote 80 wt.% LSCM–20 wt.% LDC as '80LSCM' and so on. The X-ray diffraction patterns for all of the composites exhibited peaks that corresponded to the hexagonal phase of LSCM perovskite and that were consistent with the patterns previously reported for LSCM [4,25]. The LDC ($La_{0.2}Ce_{0.8}O_{2-\delta}$) diffraction peaks corresponded to the cubic fluorite structure of ceria (JCPDF Card no. 340394). In the case of the composites, the peaks corresponding to both LSCM and LDC patterns were visible. In the XRD patterns, there was a direct correspondence between peak height and the composition of the composite (e.g., the higher the peak, the higher the LDC content of the composite). XRD analysis also revealed that the as-synthesized composite powders were highly crystalline without any impurities. The crystallite size of 100LSCM, 80LSCM, 66LSCM, 50LSCM, 33LSCM, and pure LDC was calculated as 23, 22, 21.9, 20.2, 20.1, and 13 nm, respectively, using Scherrer's formula. The specific surface area values of the composite anodes are listed in Table 1. The specific surface area increased gradually with LDC amount, within the LSCM percolation limit and then decreased at the large amount of LDC.

The morphology of each composite powder is shown in Fig. 3. Pure LSCM powder, shown in Fig. 3(a), was spherical and slightly agglomerated, whereas the LDC powder (Fig. 3(f)) was highly porous, as we reported in a previous study [26]. As the amount of LDC in the composite increased, the particle size decreased. Together, these results indicate that the sucrose modified sol–gel combustion method is very effective for the synthesis of LSCM–LDC composites.

The XRD patterns of physical mixtures of LSCM with YSZ and GDC powders after firing at 1250 °C for 5 h are shown in Fig. 4. All peaks corresponded to either the LSCM–LDC composite phase or the YSZ and GDC phases, without any impurities. The XRD data indicates that the composite is decisively compatible and chemically and thermodynamically stable with YSZ and GDC electrolytes. Moreover, the LSCM–LDC composite anode materials did not show chemical decomposition or any impurity phases after exposure to CH_4 at 800 °C for 8 h.

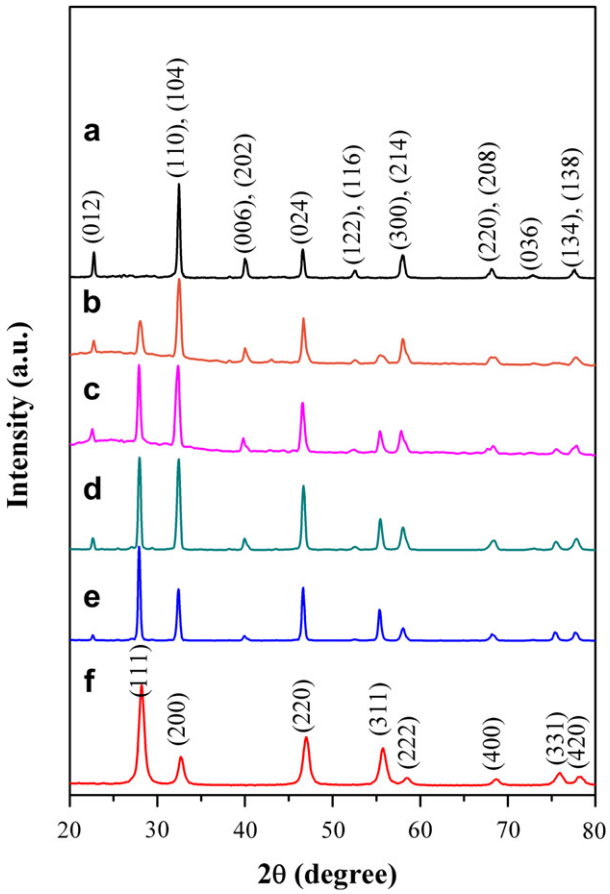

Fig. 2. XRD patterns of the as-synthesized LSCM–LDC composite powders of (a) 100 wt.% LSCM, (b) 80 wt.% LSCM–20 wt.% LDC, (c) 66 wt.% LSCM–33 wt.% LDC, (d) 50 wt.% LSCM–50 wt.% LDC, (e) 33 wt.% LSCM–66 wt.% LDC, and (f) pure LDC, calcined at 1000 °C.

3.2. Carbon deposition behavior

The carbon deposition rate was calculated from the weight loss graph based on the TGA data. Graphs of the weight change vs. temperature are shown in Fig. 5. The TGA data showed a trend of increased weight loss as the wt.% of LSCM decreased. The overall weight losses were calculated as 2.10%, 1.47%, 1.26%, 0.32%, 0.21%, and 0.03% for pure LDC, 33LSCM, 50LSCM, 66LSCM, 80LSCM, and

Table 1
Composition ratio and specific surface area of the LSCM–LDC composite anodes synthesized by a sucrose-modified sol–gel method.

Anode material	Weight of LSCM (wt.%)	Volume of LSCM (vol.%)	Specific surface area (m^2 g^{-1})
100LSCM	100	100	3.639
80LSCM	80	80.4	4.434
66LSCM	66	64.7	7.743
50LSCM	50	50.7	7.998
33LSCM	33	33.7	5.240
Pure LDC	0	0	5.790

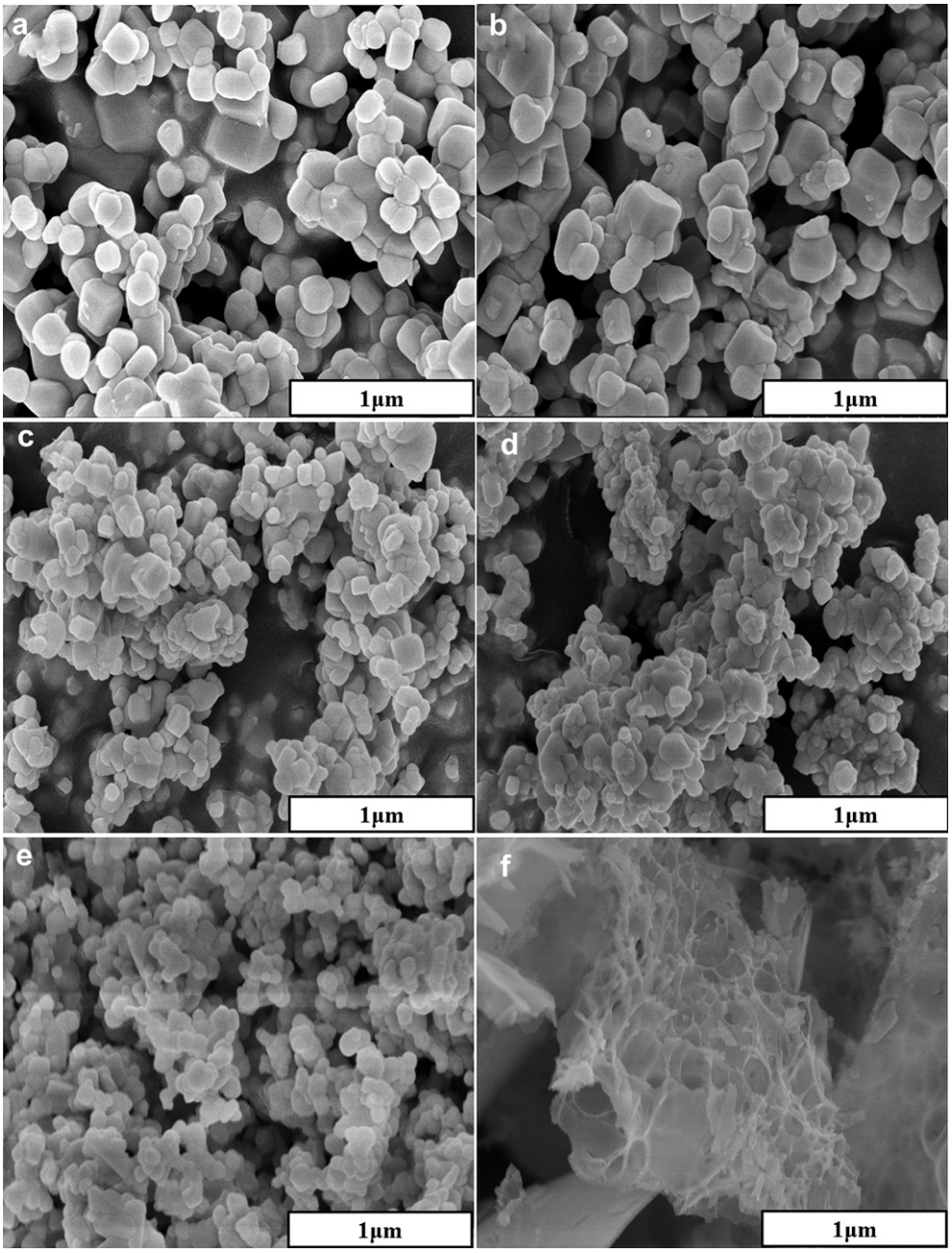

Fig. 3. FE-SEM micrographs of the as-synthesized LSCM–LDC composite powders of (a) 100 wt.% LSCM, (b) 80 wt.% LSCM–20 wt.% LDC, (c) 66 wt.% LSCM–33 wt.% LDC, (d) 50 wt.% LSCM–50 wt.% LDC, (e) 33 wt.% LSCM–66 wt.% LDC, and (f) pure LDC, calcined at 1000 °C.

100LSCM, respectively. This weight loss is due to the oxidation of the carbon deposits. Interestingly, in the samples containing LSCM, weight gain occurred in the temperature range of 300 °C–450 °C. The average weight gain values measured in composite samples were 0.1%, 0.2%, and 0.5% for 66LSCM, 80LSCM, and pure LSCM, respectively. This weight gain may be attributed to the gain of specific amounts of oxygen. Tao and Irvine reported that when reduced LSCM ($La_{0.75}Sr_{0.25}Cr_{0.5}Mn_{0.5}O_{3-\delta}$) was subjected to re-oxidation, there was a certain amount of weight gain depending upon the oxygen stoichiometry of the LSCM perovskite due to oxygen consumption [4]. However, there is no weight gain observed in the LDC during the re-oxidation process during the TGA analysis. In the LDC crystals, the cerium ion has the ability to transition between Ce^{4+} to Ce^{3+}, depending on the ambient oxygen partial pressure, while La^{3+} remains the same, in an oxidizing, as well as reducing atmosphere. Hence, it is expected that the re-oxidation process accumulates some oxygen into the reduced $La_{0.2}Ce_{0.8}O_{2-\delta}$.

Meanwhile, it has been demonstrated that CH_4 undergoes a solid–gas reaction on the surface of CeO_2 (ceria). It reacts with CeO_2 to produce CO and H_2. This solid–gas reaction involves various intermediate surfaces of the hydrocarbon species in both dry and humidified CH_4 [27,28]. The high CH_4 decomposition activity on LDC is due to the specific ability of LDC to store and release oxygen under a wide range of oxygen partial pressures and temperatures. In contrast, pure LSCM has a very poor CH_4 reaction activity [22,29]. Consequently, we expected that the LSCM–LDC composites would show better catalytic activity than LSCM despite the higher carbon deposition rate of the composite compared to pure LSCM.

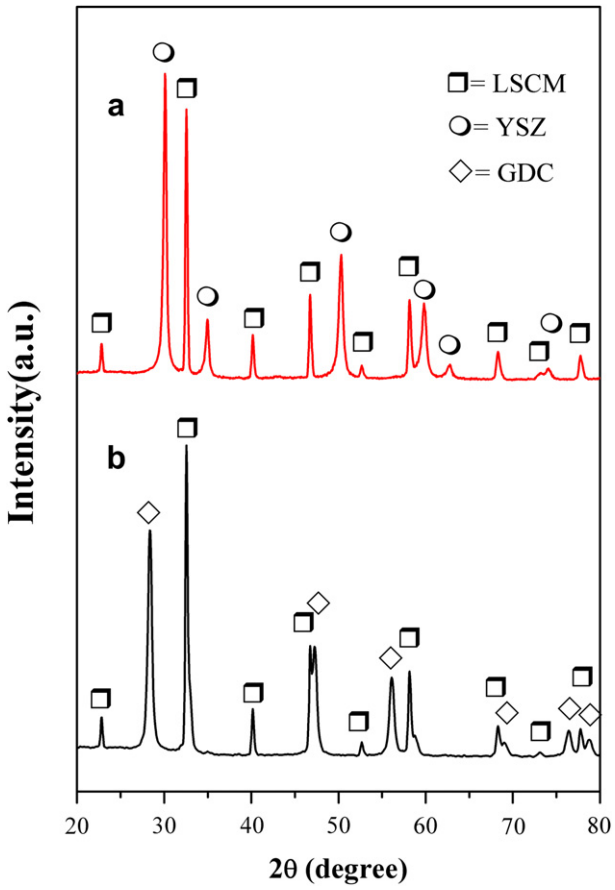

Fig. 4. XRD patterns of the physical mixtures of LSCM with (a) YSZ and (b) GDC after firing at 1250 °C for 5 h in air.

3.3. Electrochemical properties of the composites

The catalytic activity of the composites was studied by both AC impedance spectroscopy and *I*–*V* measurements of single cells. The AC impedance spectra of the LSCM–LDC composites anode in H_2 and CH_4 are shown in Fig. 6, and the calculated anode polarization resistance values at 800 °C, 750 °C, and 700 °C are provided in Table 2. While pure LSCM (100LSCM) had an anode polarization resistance, R_p, of 0.247 Ω cm^2, the R_p of the other LSCM–LDC composites in H_2 decreased linearly as the LDC content of the composites increased up to 50 wt.% LDC and then increased at the 33LSCM composition (67 wt.% LDC). The 50LSCM anode showed the lowest R_p value of 0.081 Ω cm^2 at 800 °C. The R_p in humidified CH_4 followed the same trend as that observed in humidified H_2. The R_P of 50LSCM in CH_4 at 800 °C was 0.130 Ω cm^2, which was the lowest polarization resistance for all of the composite anodes and the pure LSCM anode. Although LDC can provide catalytic activity, the 33LSCM anode, which is comprised of a large amount of LDC, exhibited higher R_p in both H_2 and CH_4 than the 50LSCM. This finding may be attributed to the low electrical conductivity of LDC, consequently leading to a slow charge transfer reaction. After AC

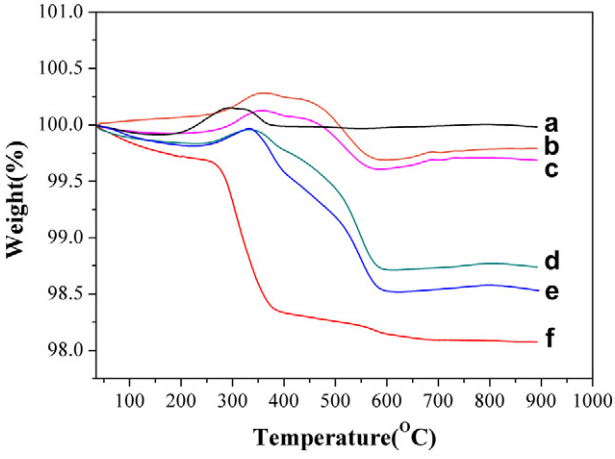

Fig. 5. TGA data of the LSCM–LDC composite powders of (a) 100 wt.% LSCM, (b) 80 wt.% LSCM–20 wt.% LDC, (c) 66 wt.% LSCM–33 wt.% LDC, (d) 50 wt.% LSCM–50 wt.% LDC, (e) 33 wt.% LSCM–66 wt.% LDC, and (f) pure LDC, exposed to CH_4 at 750 °C for 6 h.

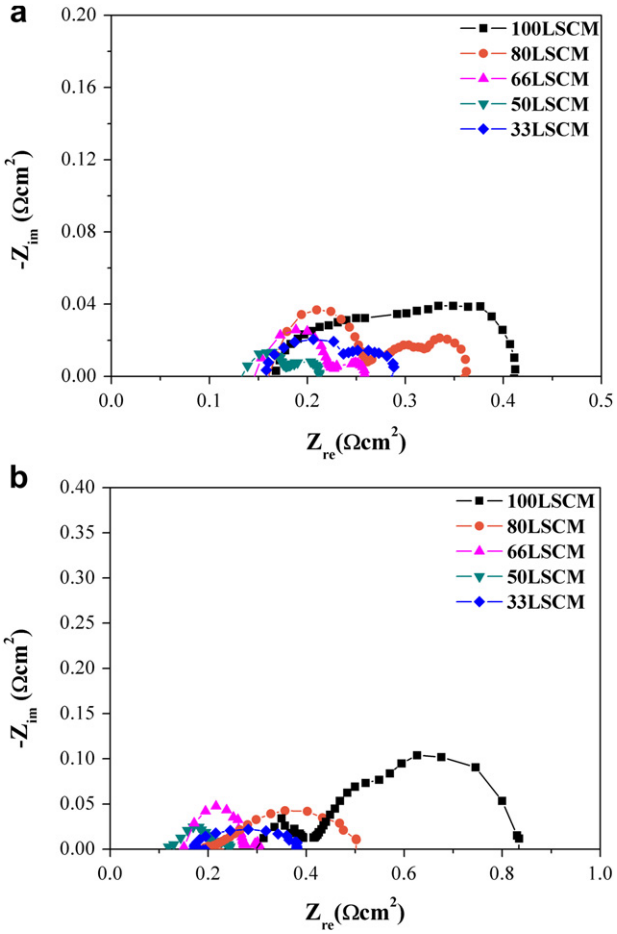

Fig. 6. Typical AC impedance spectra of the LSCM–LDC composite anodes measured at 800 °C in humidified (a) H_2 and (b) CH_4.

Table 2
Polarization resistance of the LSCM–LDC composite anodes at various operating temperatures in humidified H_2 and CH_4 fuels.

Anode material	Polarization resistance (Ω cm^2)				
	800 °C in H_2	800 °C in CH_4	800 °C after recovery	750 °C in H_2	700 °C in H_2
100LSCM	0.247	0.540	0.398	0.750	1.270
80LSCM	0.200	0.304	0.225	0.400	0.567
66LSCM	0.133	0.155	0.199	0.243	0.395
50LSCM	0.081	0.130	0.084	0.173	0.212
33LSCM	0.133	0.240	0.325	0.310	0.470

impedance spectroscopy measurements in CH_4, the cells were fed with H_2 for 2 h to investigate the redox stability of the composite anodes at 800 °C. The calculated R_p values of these composite anodes are also provided in Table 2. The recovery R_p values of 100LSCM, 80LSCM, 66LSCM, 50LSCM, and 33LSCM composite anodes were 0.398 Ω cm^2, 0.225 Ω cm^2, 0.119 Ω cm^2, 0.084 Ω cm^2, and 0.325 Ω cm^2, respectively, at 800 °C. The 50LSCM anode had a recovery rate of 94%, indicating excellent redox stability. On the basis of the excellent recovery properties of the composites, it can be deduced that the bond strength of carbon to LDC is weaker than that of carbon to LSCM.

From the above results, it is clear that the catalytic activity of the composite anodes varied according to the LDC content in the LSCM matrix. The 50LSCM composite anode demonstrated the best performance, irrespective of the operating conditions. The reasons for this result are discussed below in point form.

3.3.1. The microstructure of the composite anodes

As shown in Fig. 3, the LSCM composite possessed a very small particle size. Therefore, the 50LSCM composite anode showed better sinterability than the other composites. Moreover, the 50LSCM has the highest surface area of all anode compositions as shown in Table 1. The morphology of the as-synthesized powders can affect the final microstructure of the anodes after firing. The microstructures of the LSCM–LDC composite anodes fired at 1250 °C for 5 h are shown in Fig. 7. While the anode without LDC (100LSCM) demonstrate only point contacts between large particles and relatively poor adhesion between the anode and the electrolyte, the anode with a high LDC content showed area contact between small particles and good adhesion between the anode and electrolyte. This property resulted in lower contact and charge transfer resistance characteristics and better electrochemical performance in the anode with high LDC content.

3.3.2. Percolation limits of LDC in the LSCM matrix

According to the Kusy equation [30], the particle size ratio of LDC and LSCM determined the percolation limits of the two components:

$$\text{Percolation limit}, V_x = \frac{100}{1 + \left(\frac{\Phi}{4X_c}\right) * \left(\frac{R_p}{R_m}\right)} \quad (1)$$

where $\Phi = 1.27$ and $X_C = 0.42$ are constants for cubic packing of a square planar lattice, and R_p/R_m is the particle size ratio. For convenience and for a better approach to percolation theory, the weight ratio of the composites was converted to volume ratio using

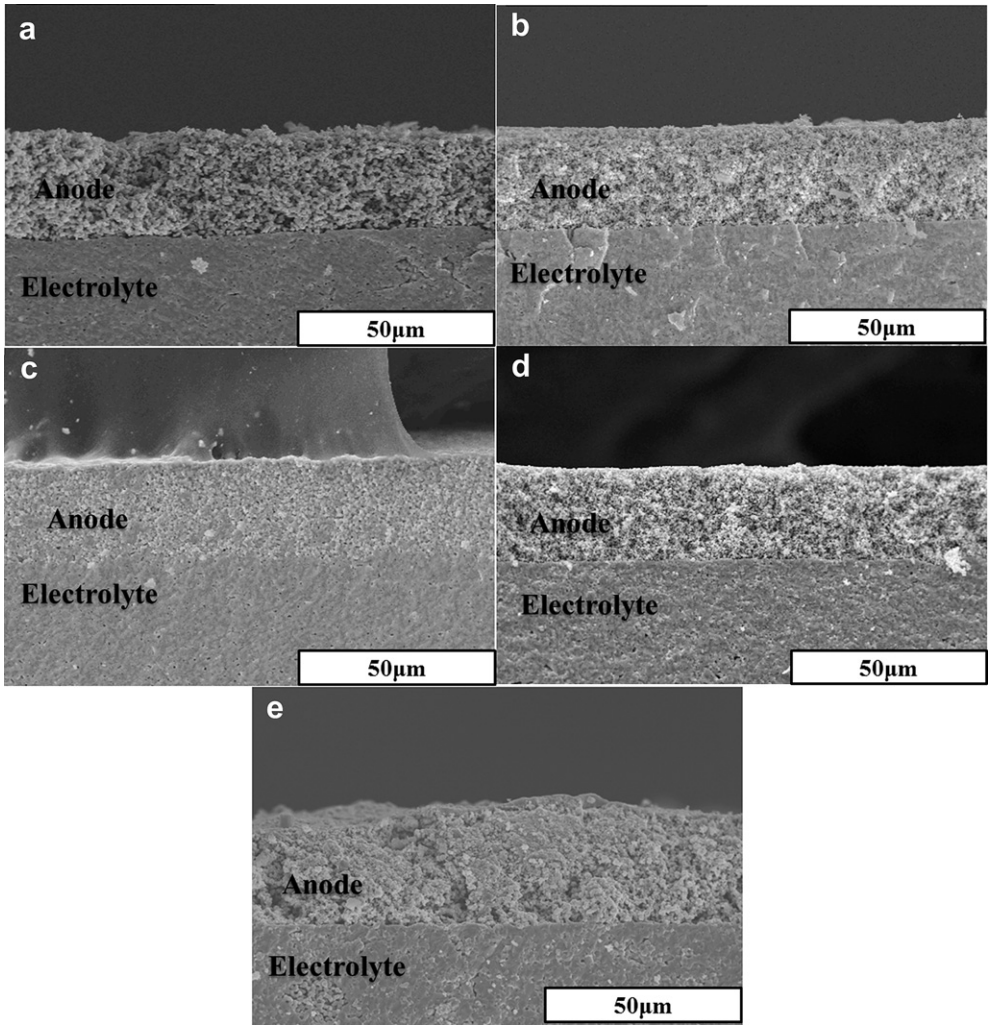

Fig. 7. Cross-sectional FE-SEM micrographs of LSCM–LDC composite anodes on GDC electrolytes after single cell measurement: (a) 100 wt.% LSCM, (b) 80 wt.% LSCM–20 wt.% LDC, (c) 66 wt.% LSCM–33 wt.% LDC, (d) 50 wt.% LSCM–50 wt.% LDC, and (e) 33 wt.% LSCM–66 wt.% LDC fired at 1250 °C for 5 h in air.

the theoretical densities of LSCM (6.68 g cm^{-3}) and LDC (6.915 g cm^{-3}) [31]. The volume ratios of the composites are listed in Table 1. The particle size of the LSCM and LDC obtained by dynamic light scattering methods was 1916.6 nm and 183.86 nm, respectively. Using Eq. (1), we calculated that the percolation limit of LDC in the LSCM matrix was 45.98 vol.% (∼50 wt.% of LDC). At this limit, LDC was thoroughly percolated into the LSCM matrix. Because LSCM is mainly an electronic conductor, the triple phase boundary (TPB), which is where reactions occur, may be limited to the interface between the LSCM and the GDC electrolyte. In LSCM–LDC composite anodes, the oxygen ion conducting LDC plays a role in the extension of the electrolyte, which could increase the TPB. Without percolation, LDC does not perform well as an extension of the electrolyte region. For the reasons described above, the 50LSCM composite anode with LDC percolation exhibited the best catalytic activity. Despite the percolation of LDC, however, the 33LSCM composite demonstrate poor electrochemical performance, due to its low electrical conductivity.

3.3.3. Effect of carbon deposition

Anode polarization resistance in a CH_4 atmosphere decreases as LDC content increases. Therefore, we expected the carbon deposition rate to increase with LDC content, which would lead to an increase in polarization resistance due to carbon coverage of reaction sites. However, we obtained the opposite results. Unlike Ni, the LSCM–LDC composites had a carbon deposition rate of less than 2%, which is insufficient to fully cover the reaction sites. This type of partial carbon coverage may provide conductive phases. Because oxide anode materials, including LSCM, usually have low electronic conductivity, conductive phases can improve the overall electrochemical performance of materials containing LSCM. It has been reported that exposure of a Cu-ceria-YSZ anode to n-butane increased the performance of the anode due to the formation of carbonaceous residues within the anode [32]. Similarly, the improvement in performance with increasing LDC content may be due to enhanced electronic conductivity within the LSCM–LDC composite anode.

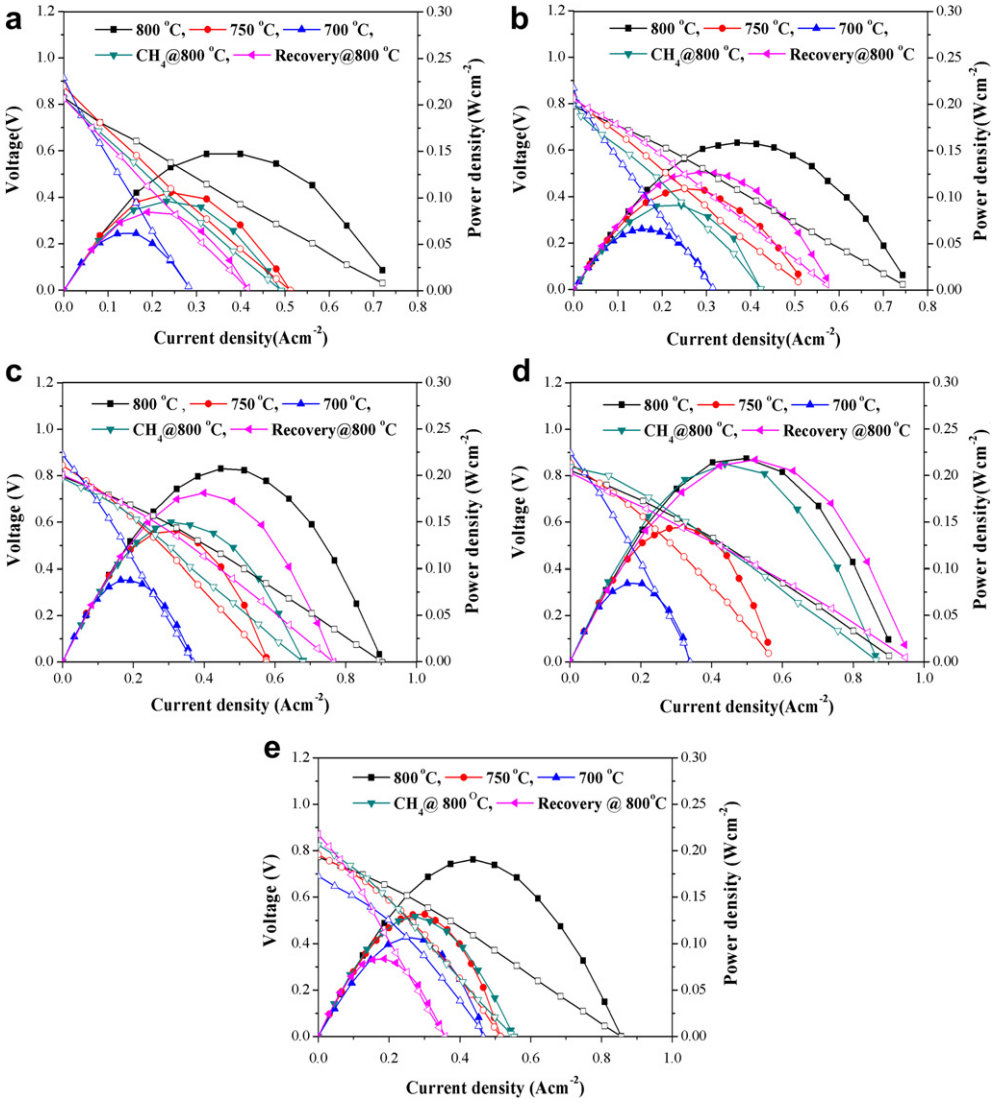

Fig. 8. Comparison of the *I–V* curves and power density of each LSCM–LDC composite anodes of (a) 100 wt.% LSCM, (b) 80 wt.% LSCM–20 wt.% LDC, (c) 66 wt.% LSCM–33 wt.% LDC, (d) 50 wt.% LSCM–50 wt.% LDC, and (e) 33 wt.% LSCM–66 wt.% LDC.

3.4. Single cell performance

The cell voltages and power density for various LSCM–LDC composite anodes, according to the operating temperature, are shown in Fig. 8. The power density decreased linearly with temperature. The maximum power densities of the 100LSCM, 80LSCM, 66LSCM, 50LSCM and 33LSCM single cells were 147 mW cm^{-2}, 160 mW cm^{-2}, 208 mW cm^{-2}, 220 mW cm^{-2}, and 192 mW cm^{-2}, respectively, under humidified H_2 at 800 °C. Hence, the power density increased with increasing LDC content, up to 50 wt.% LDC and then decreased at the 33LSCM composition (67 wt.% LDC), similar to the trend observed for catalytic activity. The changes in power density according to the LDC content in a humidified CH_4 atmosphere were consistent with the trend observed in a humidified H_2 atmosphere. The 50LSCM single cell had a much higher maximum power density of 213 mW cm^{-2} in humidified CH_4 than the 100LSCM single cell (97 mW cm^{-2}). Meanwhile, the maximum recovery power density of the 50LSCM anode, measured after re-oxidation in H_2 atmosphere, was 217 mW cm^{-2}, which demonstrates a 98% recovery rate. This is a much higher recovery rate than that reported for conventional Ni-based anodes [33]. Despite of the LDC percolation, however, the 33LSCM composite exhibited poor electrochemical performance. The poor performance may be attributed to low electrical conductivity of LDC, consequently leading to a slow charge transfer reaction.

4. Conclusions

We successfully prepared $La_{0.75}Sr_{0.25}Cr_{0.5}Mn_{0.5}O_{3-\delta}$–$La_{0.2}Ce_{0.8}O_{2-\delta}$ (LSCM–LDC) composite anodes using different weight ratios of LDC by a simple sol–gel combustion technique. The morphology of the as-synthesized composite powders could be controlled by varying the amount of LDC added to the composite. The grain growth of the LSCM matrix was likely hindered by LDC, which acted as a diffusion barrier, leading to a decrease in the particle size. The polarization of the LSCM–LDC composites in H_2 decreased with increasing LDC content because of the better microstructure and higher catalytic activity provided by LDC. Even though the carbon deposition rate increased with increasing LDC content, we observed a decrease in anode polarization resistance due to the formation of conducting carbonaceous residues within the composite anode. Finally the anode composed of 50 wt.% LDC (50LSCM), which is above the percolation limit of the LDC-dispersed LSCM matrix, showed the best electrochemical performance in both H_2 and CH_4 atmospheres.

Acknowledgments

This research was supported by a grant from the Fundamental R&D Program for Core Technology of Materials funded by the Ministry of Knowledge Economy, Republic of Korea.

References

[1] N.Q. Minh, J. Am. Ceram. Soc. 76 (1993) 563–588.
[2] S.C. Singhal, Solid State Ionics 135 (2000) 305–313.
[3] S. Tao, J.T.S. Irvine, Nat. Mater. 2 (2003) 320–323.
[4] S. Tao, J.T.S. Irvine, J. Electrochem. Soc. 151 (2004) A252–A259.
[5] X.J. Chen, Q.L. Liu, K.A. Khor, S.H. Chan, J. Power Sources 165 (2007) 34–40.
[6] J. Sfeir, J. Power Sources 118 (2003) 276–285.
[7] J. Liu, B. Madsen, Z. Ji, S. Barnett, Electrochem. Solid State Lett. 5 (2002) A122–A124.
[8] Y.H. Huang, R.I. Dass, J.C. Denyszyn, J.B. Goodenough, J. Electrochem. Soc. 153 (2006) A1266–A1272.
[9] V.V. Kharton, E.V. Tsipis, I.P. Marozau, A.P. Viskup, J.R. Frade, J.T.S. Irvine, Solid State Ionics 178 (2007) 101–113.
[10] S. Zha, P. Tsang, Z. Cheng, M. Liu, J. Solid State Chem. 178 (2005) 1844–1850.
[11] S. Tao, J.T.S. Irvine, J.A. Kilner, Adv. Mater. 17 (2005) 1734–1737.
[12] J.P. Martinez, D.M. Lopez, J.C.R. Morales, C. Savaniu, P. Nunez, J.T.S. Irvine, Chem. Mater. 18 (2006) 1001–1006.
[13] S.P. Jiang, X.J. Chen, S.H. Chan, J.T. Kwok, K.A. Khor, Solid State Ionics 177 (2006) 149–157.
[14] J. Wan, J.H. Zhu, J.B. Goodenough, Solid State Ionics 177 (2006) 1211–1217.
[15] X.J. Chen, Q.L. Liu, S.H. Chan, N.P. Brandon, K.A. Khor, J. Electrochem. Soc. 154 (2007) B1206–B1207.
[16] S. Tao, J.T.S. Irvine, Chem. Rec. 4 (2004) 83–95.
[17] S. Park, J.M. Vohs, R.J. Gorte, Nature 404 (2000) 265–267.
[18] A.L. Sauvet, J. Fouletier, F. Gaillard, M. Primet, J. Catal. 209 (2002) 25–34.
[19] A.L. Sauvet, J.T.S. Irvine, Solid State Ionics 167 (2004) 1–8.
[20] S.W. Tao, J.T.S. Irvine, Chem. Mater. 16 (2004) 4116–4121.
[21] S.P. Jiang, X.J. Chen, S.H. Chan, J.T. Kwok, J. Electrochem. Soc. 153 (2006) A850–A856.
[22] Y. Xiong, K. Yamaji, T. Horita, N. Sakai, H. Yokokawa, J. Electrochem. Soc. 151 (2004) A407–A412.
[23] T. Shimonosono, Y. Hirata, S. Sameshima, J. Am. Ceram. Soc. 88 (2005) 2114–2120.
[24] K.Q. Huang, J.H. Wan, J.B. Goodenough, J. Electrochem. Soc. 148 (2001) A788–A794.
[25] J. Peña-Martínez, D. Marrero-López, J.C. Ruiz-Morales, B.E. Buergler, P. Núñez, L.J. Gauckler, J. Power Sources 159 (2006) 914–921.
[26] M.K. Rath, S.K. Acharya, B.H. Kim, K.T. Lee, B.G. Ahn, Mater. Lett. 65 (2011) 955–958.
[27] K. Otsuka, M. Hatano, A. Morikawa, J. Catal. 79 (1983) 493–496.
[28] N. Laosiripojana, S. Assabumrungrat, Appl. Catal. B60 (2005) 107–116.
[29] J. Sfeir, P.A. Buffat, P. Möckli, N. Xanthopoulos, R. Vasquez, H.J. Mathieu, J. Van herle, K.R. Thampi, J. Catal. 202 (2001) 229–244.
[30] R.P. Kusy, J. Appl. Phys. 48 (1977) 5301–5305.
[31] E. Suda, B. Pacaud, M. Mori, J. Alloy Compd. 408–412 (2006) 1161–1164.
[32] S. McIntosh, J.M. Vohs, R.J. Gorte, J. Electrochem. Soc. 150 (2003) A470–A476.
[33] R.J. Gorte, H. Kim, J.M. Vohs, J. Power Sources 106 (2002) 10–15.